Influence of Some Test Parameters on Dry Sliding Wear Characteristics of a Zinc-11.5% Aluminum Alloy

B.K. Prasad

(Submitted 12 October 2001; in revised form 20 February 2002)

This study analyzes observations made pertaining to the sliding wear response of a Zn-11.5% Al alloy in different test conditions. The wear rate and frictional heating increased with sliding speed and pressure. Seizure pressure of the samples reduced with the test speed. Frictional heating, the severity of surface and subsurface damage, and debris size increased with speed and pressure. Sticking of debris particles on the specimen surface was noted at low sliding speed. Specimen seizure was caused by the application of high pressure in view of excessive adherence of the specimen material on to the disk surface. Considerable wear-induced subsurface deformation took place in general; the degree of deformation decreased as the depth below the wear surface increased. Wear behavior of the samples is discussed in terms of the lubricating nature and thermal stability of its various microconstituents and specific characteristics of wear surfaces, subsurface regions, and debris particles.

Keywords dry sliding wear, wear behavior, Zn-ll.5 Al alloy

1. Introduction

Zinc(Zn)-based alloys have emerged as a potential cost- and energy-effective substitute material system for various ferrous and nonferrous alloys for different engineering applications.[1-4] One of the important varieties in the category of high-strength Zn-based alloys consists of 11.0-12.0% aluminum (Al) along with copper (Cu) and magnesium (Mg). The alloy composition has been exploited considerably to establish its application potential at different levels.[1-4] However, limited efforts have been made to understand its wear response in various test conditions, especially in terms of analyzing material removal mechanisms and factors responsible for typical wear characteristics in specific situations.

In view of the above, an attempt has been made to assess the wear behavior of a Zn-based alloy containing 11.5% aluminum along with Cu and Mg. Wear surfaces, subsurface regions, and debris particles have also been characterized and their features correlated with typical wear response of the alloy in specific test conditions.

2. Experimental

2.1 Alloy Preparation

The Zn-based alloy, having a composition of 11.5% Al, 2.5% Cu, 0.04% Mg, and the balance Zn, was prepared by a liquid metallurgy route. The alloy melt was solidified in a cast iron mold in the form of 20 mm diameter × 150 mm long cylindrical castings.

B.K. Prasad, Regional Research Laboratory (CSIR), Bhopal - 462 026, India. Contact e-mail: braj_kprasad@hotmail.com.

2.2 Sliding Wear

Dry sliding wear tests were conducted at room temperature (35 °C) on 8 mm diameter × 53 mm long cylindrical pins fabricated from the alloy castings. An EN25 steel (0.3% C, 0.7% Cr, 2.5% Ni, 0.5% Mo, and the remainder Fe) disk with a hardness of Rc 32 was used as the counterface (disk). The wear test apparatus was a Cameron-Plint pin-on-disk machine (Plint Partners, Wokingham, Berkshire, UK). A schematic representation of the wear test apparatus is shown in Fig. 1. Wear tests were carried out at the sliding speeds of 0.42, 1.38, 2.68, and 4.60 m/s. Pressure was increased in steps until specimen seizure was indicated in terms of a high rate of temperature increase and material loss, large adhesion of the pin material onto the disk surface, and abnormal noise in the pin-disk assembly prior to traversing a sliding distance of 500 m. The temperature near the contacting surface of the specimens was monitored as a function of test duration by inserting a chromel-alumel thermocouple in a hole 1.5 mm away from the contacting surface of the sample. Wear rate was computed by the weight-loss technique. A Mettler microbalance (Mettler Toledo GmbH, Greifensec, Switzerland) was used for weighing the

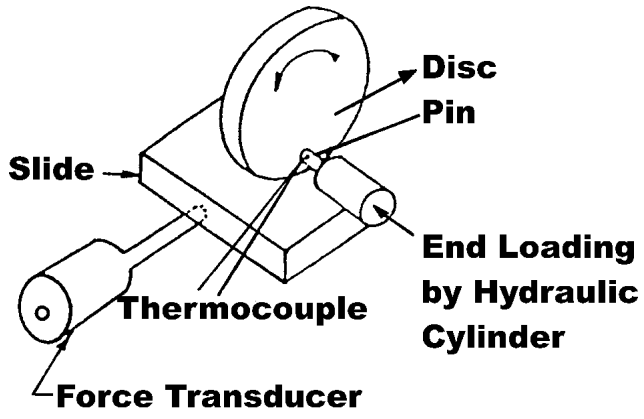

Fig. 1 Schematic representation of the wear test apparatus

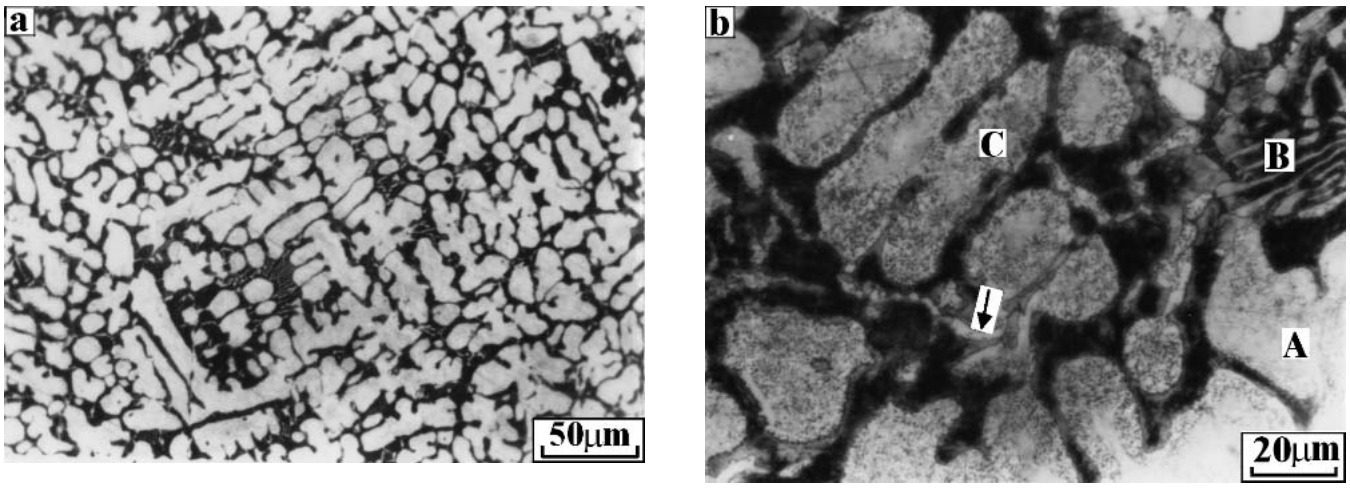

Fig. 2 Microstructure of the alloy showing **(a)** dendritic structure and **(b)** various microconstituents; A: primary α; B: eutectic α + η; C: eutectoid α + η; and arrow: ϵ

samples prior to and after the wear tests. The disk and the pin (specimen) were polished to a roughness level Ra of 0.08 μm (where Ra is the arithmetic mean of the departure of the surface roughness profile from the mean line) prior to conducting the wear tests.

2.3 Microscopy and Hardness Measurement

Microstructural observations were made on metallographically polished and etched (with diluted aqua regia) samples. Optical microscopy was used to characterize the microstructure in terms of the mode of distribution of various constituent phases. The hardness of different phases of the polished and etched samples was measured using a Leica microhardness tester (Leica Cambridge Ltd., Cambridge, UK) at an applied load of 0.10 Kg.

Wear surfaces, subsurface regions, and debris particles were analyzed with a JEOL 35CF scanning electron microscope (SEM). The samples were mounted on brass studs and sputtered with gold prior to their SEM examination. The subsurface regions were fixed in polyester resin, polished metallographically, and etched with diluted aqua regia prior to being mounted on the brass studs. The debris particles were suspended in acetone, spread on a glass plate, and placed on the studs with the help of an adhesive tape.

3. Results

3.1 Microstructure and Hardness

Figure 2 represents microstructural characteristics of the alloy. Dendritic structure (Fig. 2a) showing primary α dendrites, eutectic and eutectoid α + η, and ϵ (Fig. 2b, regions marked A, B, C, and arrow, respectively) was observed. The hardness of regions marked A, B, and C in Fig. 2(b) was HV 30, 34, and 37, respectively. The hardness of the region marked by arrow (Fig. 2b) could not be measured due to the unavailability of sufficiently wide areas (containing the phase) needed for indentation.

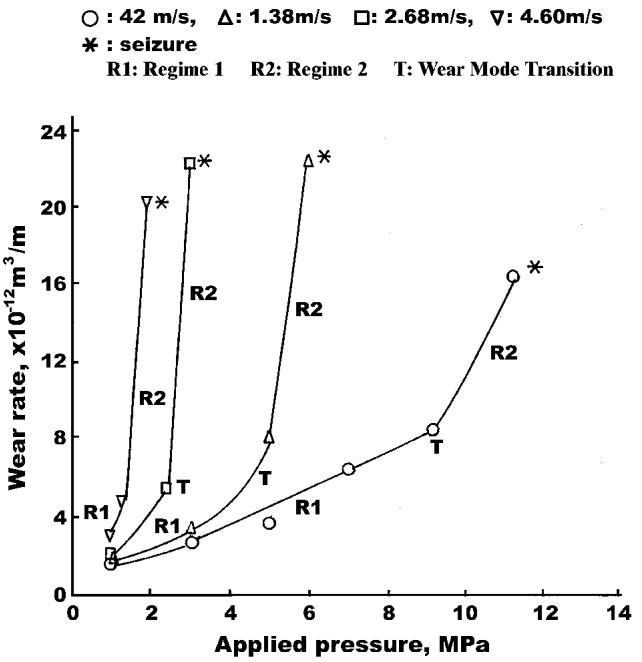

Fig. 3 Wear rate versus pressure plots of the alloy at various sliding speeds

3.2 Wear Behavior

The wear rate of the alloy was plotted as a function of applied pressure in Fig. 3. The effect of sliding speed on the wear behavior is also shown in the figure. Wear rate increased with pressure and speed. The wear rate versus pressure plots showed two regimes in general wherein the slope was low initially (regime 1) followed by a higher slope (regime 2) beyond a specific pressure, termed the transition pressure. The slope of regime 1 increased with sliding speed (Fig. 4). A similar trend was also observed for the slope of regime 2 up to the sliding speed of 2.68 m/s. The increase in slope of regime 2 became practically insensitive to speed beyond 2.68 m/s. The

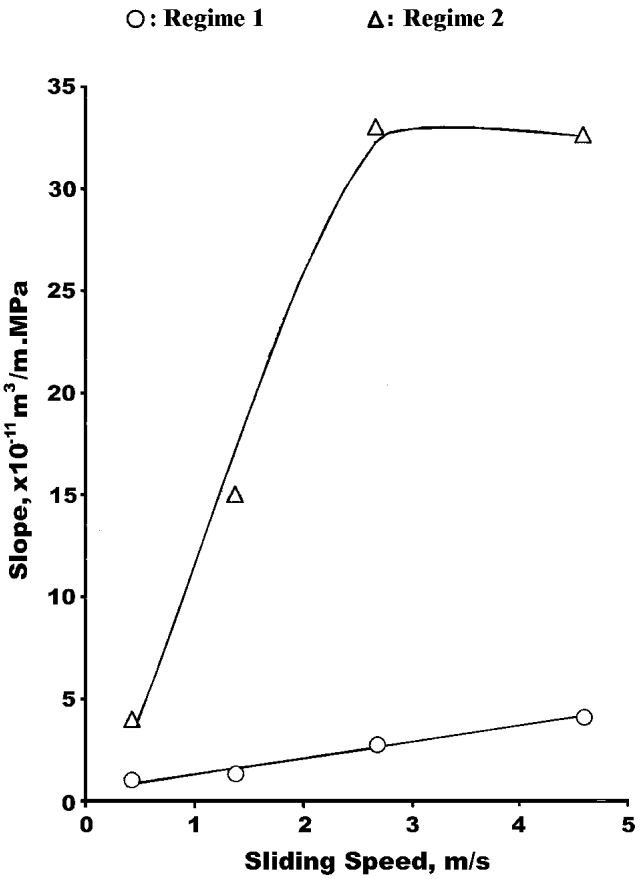

Fig. 4 Slopes of the two regimes of the wear rate versus pressure plots as a function of sliding speed

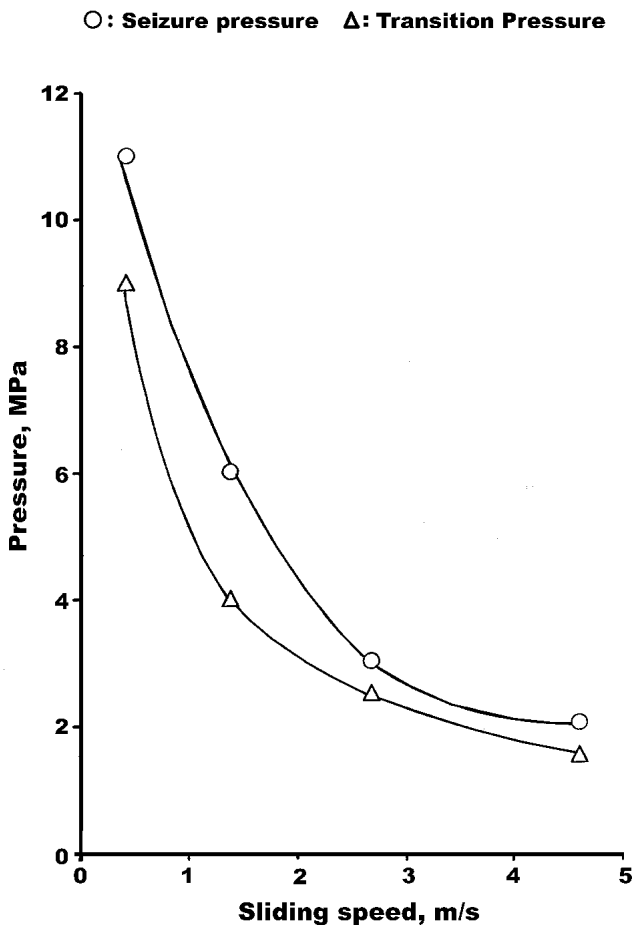

Fig. 5 Seizure and transition pressures plotted as a function of sliding speed

(transition) pressure, at which the change in slope was observed, reduced with sliding speed (Fig. 5). The seizure pressure also decreased with speed (Fig. 5).

The temperature near the specimen surface versus test duration plots at different sliding speeds are shown in Fig. 6. The influence of applied pressure can also be visualized in the figure. The temperature increased with test duration and pressure. At low applied pressures, the rate of temperature increase was high initially. This was followed by a lower rate of increase in temperature at longer test durations. At high applied pressures, the rate of temperature increase was the least in the intermediate test intervals of 250-500, 150-250, 25-100, and 20-50 s at the sliding speeds of 0.42, 1.38, 2.68, and 4.60 m/s respectively, (Fig. 6a-d). This was followed once again by a higher rate of temperature increase toward the end of the tests.

Maximum temperature near the specimen surface is shown as a function of applied pressure at different speeds in Fig. 7. The frictional heating increased with pressure and speed. Moreover, the (maximum) temperature versus pressure plots assumed two slopes at lower speeds wherein the slope was less at low pressures, followed by a higher slope beyond a critical pressure; the critical pressure reduced with test speed. Testing at higher speed caused the data plots to attain one slope only. This was comparable to that of the higher slope attainable at lower speeds.

3.3 Wear Surfaces

Figure 8 shows wear surfaces of the alloy in different test conditions. Testing at low pressures generally revealed smooth wear surfaces (Fig. 8a,d) with a few deeper grooves (Fig. 8a, region marked by arrow). The severity of surface damage increased with pressure (Fig. 8c versus a) and speed (Fig. 8d versus a). Sticking of debris and its smearing on the wear surfaces was also observed (Fig. 8b, region marked A). Seizure caused severe surface damage (Fig. 8c,e).

3.4 Subsurface Regions

Subsurface regions of the samples tested in different test conditions are shown in Fig. 9. The degree of deformation decreased with increasing depth of the region below the wear surface (top). Greater depth of deformation was noted with increasing pressure (Fig. 9c versus b). Moreover, the severity of deformation became more with increasing speed (Fig. 9f versus c). Three distinct regions could be observed in the subsurface regions namely (1) the one in the near vicinity of wear surface (top) which was subjected to maximum deformation and comprised of extremely fine microconstituents (region marked A); (2) the region (below the first one) showing flow of microconstituents in sliding direction (region marked B);

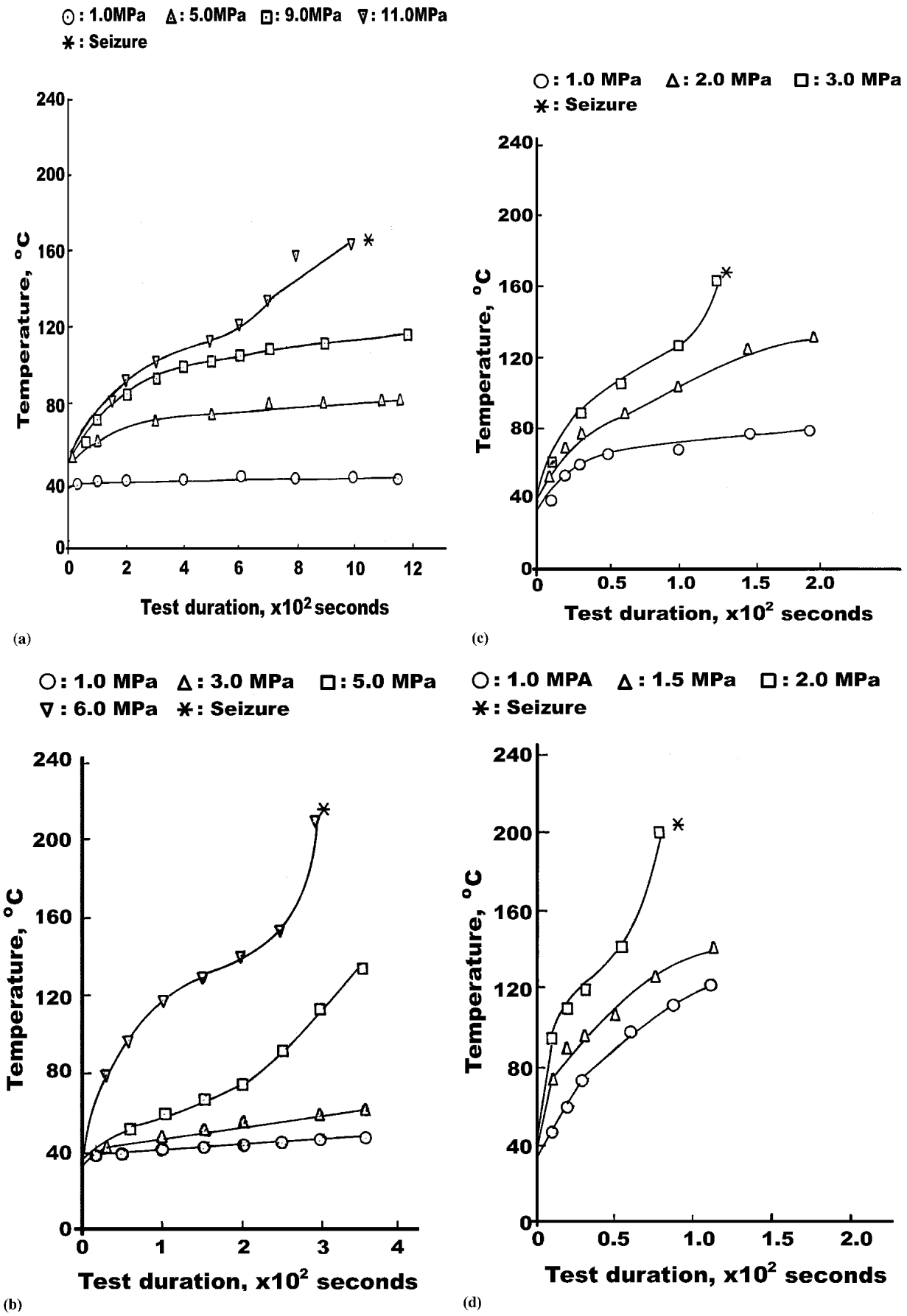

Fig. 6 Temperature near the specimen surface plotted as a function of test duration at various pressures at the sliding speeds of **(a)** 0.42 m/s, **(b)** 1.38 m/s, **(c)** 2.68 m/s, and **(d)** 4.60 m/s

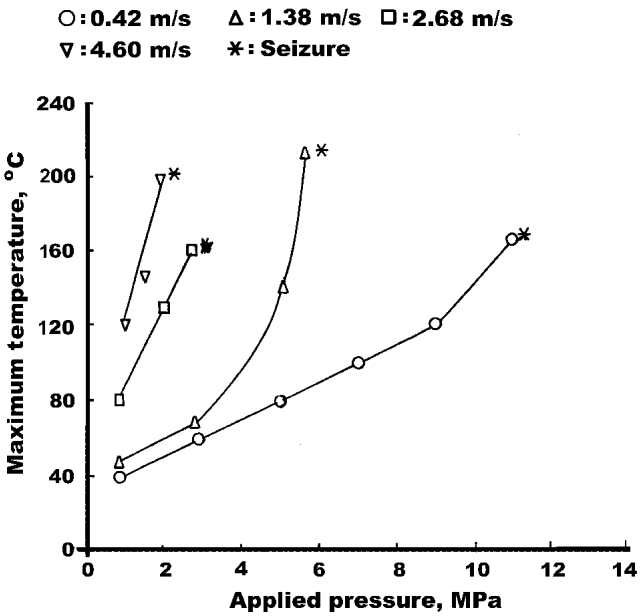

Fig. 7 Maximum temperature near the specimen surface plotted as a function of applied pressure at different speeds

and (3) the unaffected bulk structure (region marked C). Microcracks were also observed in general (arrow marked regions).

3.5 Wear Debris

The debris particles of the samples are shown in Fig. 10. In general, flaky particles were observed in the debris along with a few machining chips (Fig. 10b, regions marked by A and single arrow, respectively). The debris became coarser with increasing test pressure (Fig. 10b versus a, and 10d versus c) and speed (Fig. 10d versus b). Microcracks were also observed in the debris (Fig. 10d, region marked by double arrow).

4. Discussion

The Zn-based alloy in this study was composed of 11.5% Al, 2.5% Cu, and 0.04% Mg. Cu, when present in quantities greater than 1%, forms metastable ϵ phase,[5,6] while Mg goes to solid solution in the alloy system.[7] A eutectic reaction takes place at 382 °C when the alloy contains 5.0% Al. This causes the formation of eutectic $\alpha + \eta$.[8] Similarly, a eutectoid reaction occurs at 275 °C in the alloy consisting of 22% Al forming eutectoid $\alpha + \eta$.[8] Localized segregation of Al during solidification is very common in the alloy system in view of its wide freezing range and large difference in the density of Al and Zn. This leads to the occurrence of eutectic as well as eutectoid transformations together, depending on the localized concentration of Al in the solidifying alloy melt.[9] In view of this, the alloy contained primary α dendrites, eutectic and eutectoid $\alpha + \eta$, and metastable ϵ phase (Fig. 2b, regions marked by A, B, C and arrow respectively). The α and η phases are solid solutions of Zn and Al, in Al and Zn, respectively. The α phase imparts load-bearing and deformability characteristics.[10] The face-centered-cubic (fcc) crystal structure of the α phase enables it to offer good deformability characteristics. Face-centered-cubic crystals are known to have the maximum number of slip systems, ie., the number of (close-packed) slip planes multiplied by the number of (closed-packed) slip directions, leading to their high deformability characteristics.[11] The η phase has hexagonal crystal structure with a larger *c/a* ratio of 1.855 than that of an ideal close-packed hexagonal (cph), i.e., 1.633.[12] Phases or materials with higher *c/a* ratio than that of an ideal cph are known to possess good smearing tendency along their basal planes and thereby offer solid lubrication characteristics.[13,14] Accordingly, the η phase acts as a solid lubricant.[10] It also offers load-bearing capability to the alloy system.[10] The ϵ phase is a relatively harder microconstituent and exhibits wear resistance.[15,16] However, the alloy system has low melting characteristics as a whole. Accordingly, its properties deteriorate very fast at temperatures above ~120 °C[2], and hence the phases play their mentioned positive roles more effectively only at low operating temperatures.

Deteriorating wear performance of the alloy with increasing speed and pressure (Fig. 3 and 5) was attributed to its inferior elevated temperature properties, and this attribute is substantiated through high frictional heating experienced by the samples under the circumstances (Fig. 6 and 7). Seizure (Fig. 3) took place due to excessive frictional heating (Fig. 6 and 7) as a result of severe wear conditions generated at high speed/pressure. Under the circumstances, excessive adhesion of the specimen material onto the disk surface takes place,[17] leading to high wear rates (Fig. 3). Severe surface damage (Fig. 8c,e) and coarse debris formation (Fig. 10b,d) also agreed with high wear rates. On the contrary, low wear rates (Fig. 3) were characterized by the generation of less frictional heat (Fig. 6 and 7), fewer damaged wear surfaces (Fig. 8a,d), and finer debris formation (Fig. 10a,c). Different slopes in the wear rate and temperature versus pressure plots (Fig. 3 and 7) suggest changing wear mechanisms from mild wear (low slope) to severe wear (high slope).

Initially a high rate of temperature increase with test duration (Fig. 6) could be attributed to the abrasive action caused by the hard particles entrapped in between the mating surfaces.[18] Such hard particles are basically oxides of the contacting surface materials generated as a result of the fragmentation of the initially contacting asperities due to excessive stressing.[19] It may be noted in this context that the initial contact between the mating surfaces takes place on a very limited number of highly protruding asperities.[20] The asperities are the ones to effectively carry the entire applied load. Accordingly, they are highly stressed, leading to their yielding and subsequent fragmentation and oxidation during sliding.[18,21] The so-generated oxide particles are hard and thus abrade the specimen surface on their entrapment, as discussed earlier. In due course of time, the effective contacting surface area increases, causing the stress level to reduce. Mild wear condition is generated in such cases in view of the increased probability of the formation of lubricating films of the Zn-rich η phase. This causes a reduced rate of frictional heating at longer test durations (Fig. 6). A higher rate of frictional heating toward the final stage of wear testing could be a result of the large extent of material adhesion on to the disk surface[17] due to the destruction of the lubricating films formed earlier.[19]

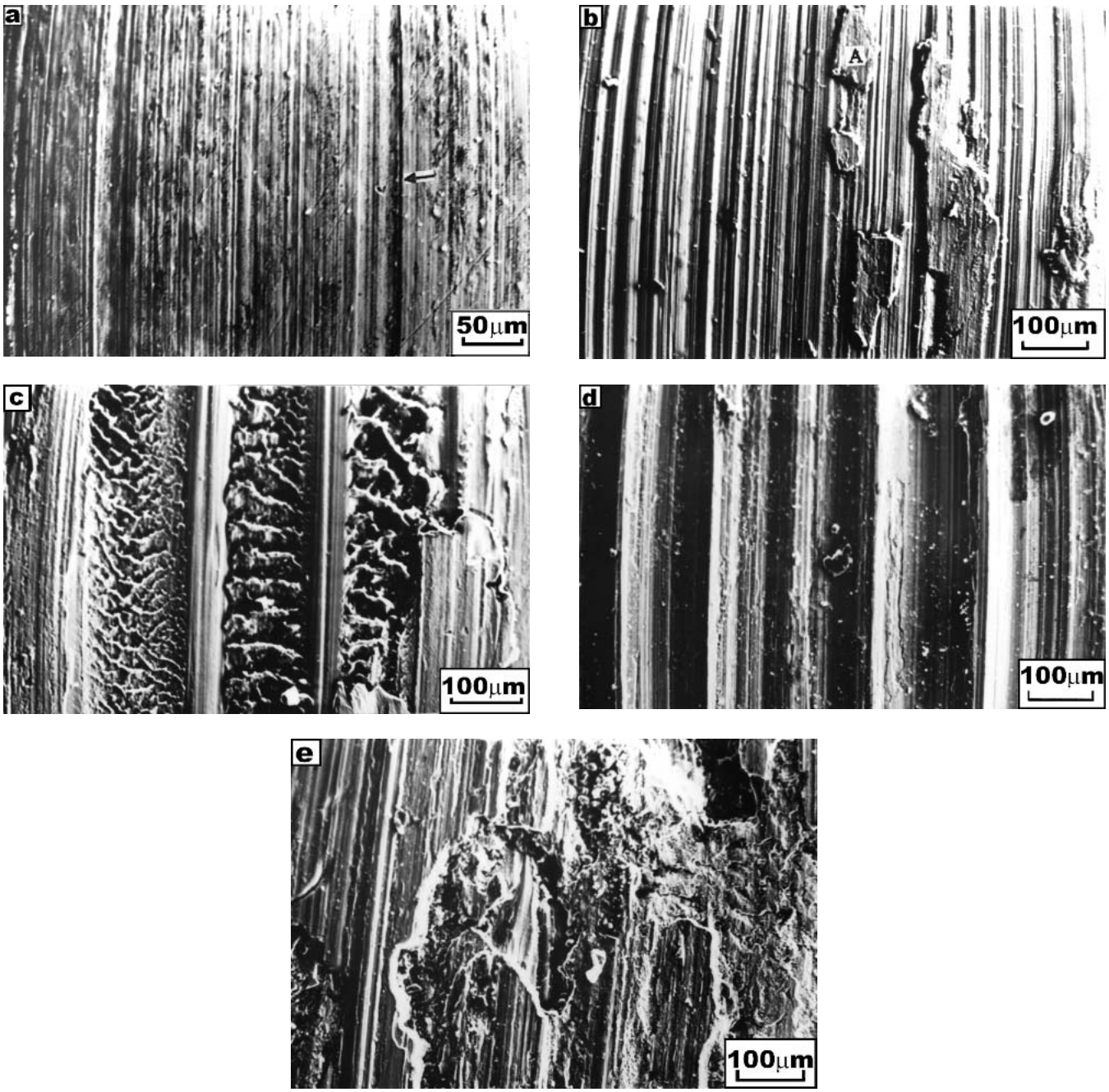

Fig. 8 Wear surfaces of the samples tested at the speeds of **(a-c)** 0.42 m/s and **(d,e)** 4.60 m/s at the pressures of (a,d) 1.0 MPa, (b) 7.0 MPa, (c) 11.0 MPa, and (e) 2.0 MPa. Arrow: deeper wear groove and A: sticking of debris on the wear surface

Differential microstructural features of the regions below the wear surfaces (Fig. 9) result from a varying degree of deformation and straining that the regions experience during wear.[22,23] The higher the degree of deformation, the finer the microconstituents in view of increased dislocation density of the affected regions.[24] The region nearest the wear surface undergoing maximum deformation exhibited the finest microconstituents (Fig. 9, regions marked A). The region (marked B in Fig. 9) below the one marked A experienced less severity of deformation leading to the flow of microconstituents in the direction of sliding. The unaffected region farthest from the wear surface (Fig. 9, region marked C) underwent no deformation leading to the exhibition of original bulk structure similar to Fig. 2.

5. Concluding Remarks

An appraisal of observations made in this investigation suggests deteriorating wear performance of the alloy with increas-

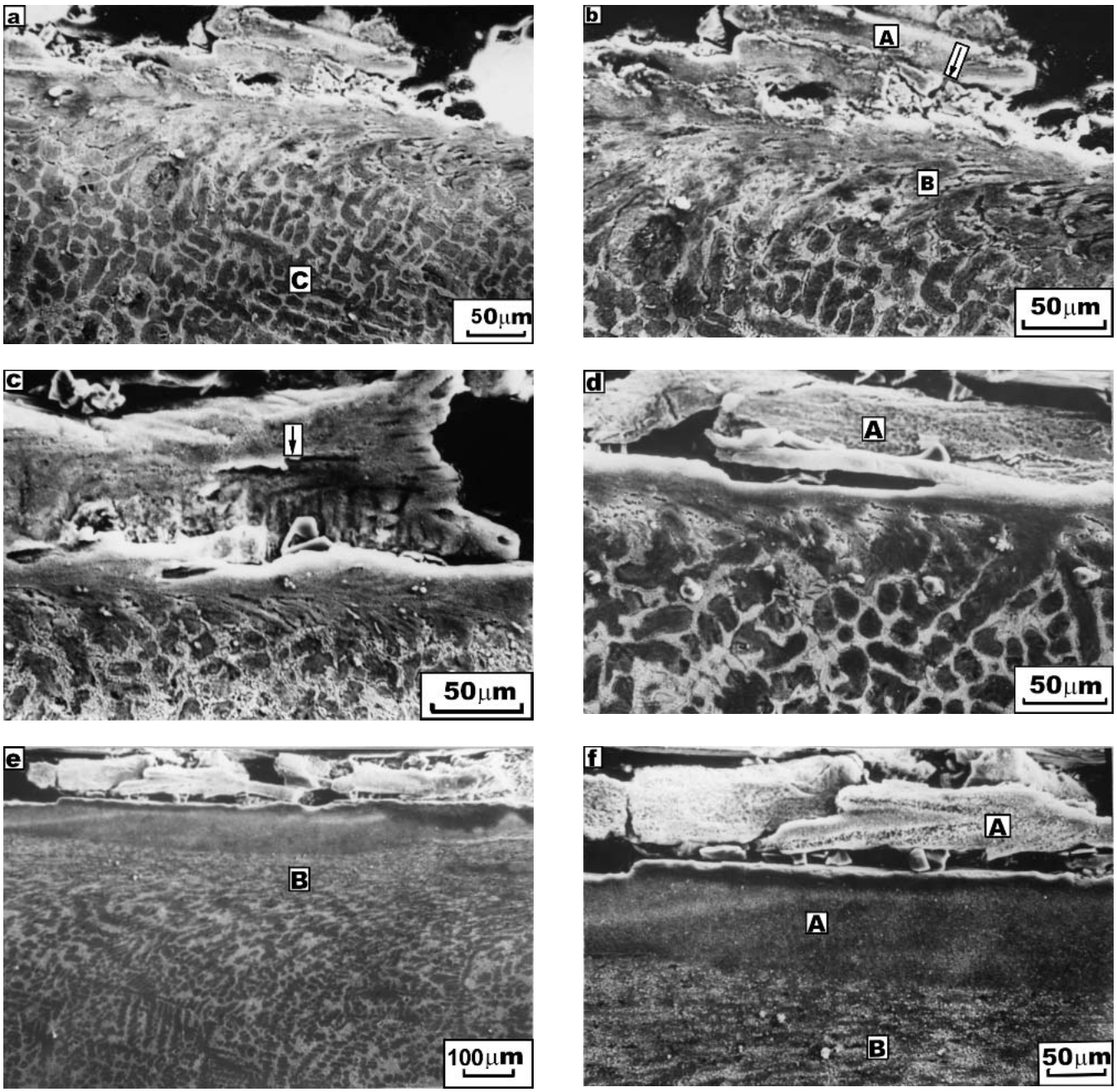

Fig. 9 Subsurface regions of the alloy tested at the sliding speed of (a-c) 0.42 m/s and (d-f) 4.60 m/s at the pressure of (a,b,d) 1.0 MPa, (c) 11.0 MPa, and (e,f) 2.0 MPa. A: heavily deformed region showing finest microstructure; B: flow of microconstituents in sliding direction; C: unaffected bulk; arrow: microcracks

ing test pressure and speed. Higher wear rates of the samples agreed with high frictional heating, more severe surface damage, and coarser debris formation. Low melting characteristics of microconstituents of the alloy significantly deteriorated the wear behavior of the samples at high speeds and pressures. The initially low slope of the wear rate versus pressure plots suggests the occurrence of mild wear at low pressures, whereas a higher slope at large applied pressures corresponds to severe wear. Adhesion was the dominant mechanism of material removal; abrasion played only a secondary role.

References

1. T.S. Calayag: "Zinc Alloys Replace Bronze in Mining Equipment Bushings and Bearings," *Mining Eng.,* 1983, *35,* pp. 727-28.
2. E.J. Kubel Jr.: "Expanding Horizons for ZA Alloys," *Adv. Mater. Process.,* 132(1987) 51-57.
3. G.C. Pratt: "Materials for Plain Bearings," *Int. Mater. Rev.,* 1973, *18,* pp. 1-27.
4. E. Gervais, H. Levert, and M. Bess: "Development of a Family of Zinc Base Foundry Alloys," *Trans. AFS,* 1980, *68,* pp.183-94.
5. E. Gervais, R.J. Barnhurst, and C.A. Loong: "An Analysis of Selected Properties of ZA Alloys," *J. Met.,* 1985, *37*, pp. 43-47.

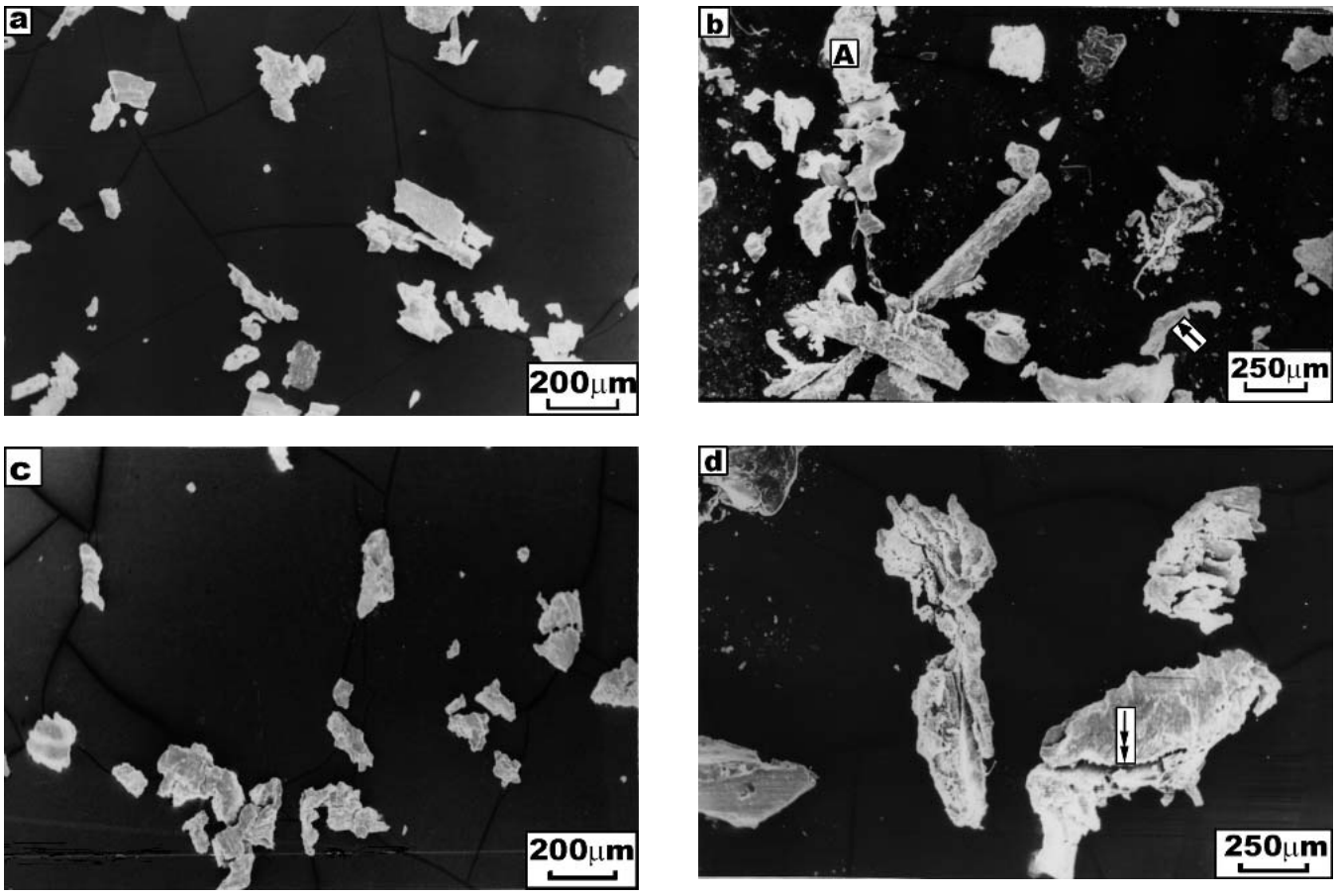

Fig. 10 Wear debris of the alloy tested at the speeds of **(a,b)** 0.42 m/s and **(c,d)** 4.60 m/s at the pressure of (a,c) 1.0 MPa, (b) 11.0 MPa, and (d) 2.0 MPa. A: flake; single arrow: machining chip; and double arrow: microcracks

6. G. Walmag, M. Lamberights, and D. Guetsouradis: "The Effects of Processing Conditions on the Microstructure and Mechanical Properties of ZA 27" in *Proc. Int. Conf. Cast Zinc-Aluminum (ZA) Alloys,* 25th Annual Conference of Metallurgists, G.P. Lewis, R.J. Barnhurst and C.A. Loong, eds., Metallurgical Society of Canadian Institute of Metals, Toronto, Ontario, Canada, 1986, pp. 5-22.
7. L.A.J. Lodder: "Zinc-Based Alloys" in *Non-Ferrous Foundry Metallurgy,* 1st ed., A.J. Murphy, ed., McGraw Hill, 1954, pp. 445-62.
8. G.R. Godlak and J. Gordan: "A High Temperature X-ray Diffractometer Study of the Zinc-Aluminium in the Region 40-75 wt% Zinc," *J. Inst. Met.,* 1963-64, *92,* pp. 230-33.
9. B.K. Prasad: "Influence of Heat Treatment on the Physical, Mechanical and Tribological Properties of a Zinc-Based Alloy," *Z. Metallkde.,* 1996, *87,* pp. 226-32.
10. S. Murphy and T. Savaskan: "Comparative Wear Behaviour of Zn-Al Based Alloys in an Automotive Engine Application," *Wear,* 1984, *98,* pp. 151-61.
11. Anon: "Plastic Deformation of Single Crystals," *Mechanical Metallurgy,* 2nd ed., G.E. Dieter, ed., McGraw Hill, 1983, pp. 105-49.
12. Anon: "The Physical Metallurgy of Zinc" in *Zinc and Its Alloys and Compounds,* 1st ed., S.W.K. Morgan, ed., Ellis Horwood, John Willey & Sons, New York, NY, 1985, pp. 154-64.
13. E.R. Braithwaite and G.W. Rowe: "Principles of Lubrication With Solids," *Sci. Lubr.,* 1963, pp. 92-100.
14. T. Tsuya and R. Takagi: "Lubricating Properties of Lead Films on Copper," *Wear,* 1964, *7,* pp. 131-43.
15. R.J. Barnhurst and J.C. Farge: "Evaluation of ZA12 and ZA27 for Bearing Applications," *Proc. Int. Conf. Cast Zinc-Aluminum (ZA) Alloys,* 25th Annual Conference of Metallurgists, G.P. Lewis, R.J. Barnhurst and C.A. Loong, ed., Metallurgical Society of Canadian Institute of Metals, Toronto, Ontario, Canada, Aug. 17-20, 1986, pp. 85-105.
16. T.J. Risdon, W.M. Mihaichuk, and R.J. Barnhurst: "Comparative Wear Rate Evaluation of Zinc-Aluminium (ZA) and Bronze Alloys Through Block-On-Ring Testing and Field Applications" in *Proc. Int. Congr. Expo,* SAE, Feb. 24-28, 1986, Detroit, Michigan, Paper No. 860064.
17. B.K. Prasad, A.K. Patwardhan, and A.H. Yegneswaran: Wear Characteristics of a Zinc-Based Alloy Compared With a Conventional Bearing Bronze Under Mixed Lubrication Condition: Effects of Material and Test Parameters," *Can. Metall. Quart.,* 2001, *40,* pp. 190-207.
18. O.P. Modi, B.K. Prasad, A.H. Yegneswaran, and M.L. Vaidya: "Dry Sliding Wear Behaviour of Squeeze Cast Aluminium Alloy-Silicon Carbide Composites," *Mater. Sci. Eng. A,* 1992, *151A,* pp. 235-45.
19. B.K. Prasad, A.K. Patwardhan, and A.H. Yegneswaran: "Factors Controlling the Dry Sliding Wear Behaviour of a Leaded-Tin Bronze," *Mater. Sci. Technol.,* 1996, *12,* pp. 427-35.
20. F.E. Kennedy, Jr.: "Thermal and Thermo-Mechanical Effects in Dry Sliding," *Wear,* 1984, *100,* pp. 453-76.
21. J.P. Pathak and S.N. Tiwari: "On the Mechanical and Wear Properties of Copper-Lead Alloys," *Wear,* 1992, *155,* pp. 37-47.
22. J. Larsen-Badse and K.G. Mathew: "Influence of Structure on the Abrasion Resistance of 1040 Steel," *Wear,* 1969, *14,* p. 199.
23. J. Larsen-Badse: "Role of Microstructure and Mechanical Properties in Abrasion," *Scripta Metall.,* 1990, *24,* pp. 821-26.
24. W.A. Glaeser: "High Strain Mechanisms in Ferrous Alloys," *Wear,* 1988, *123,* pp. 155-69.